Simulations of single and two-component galaxy decompositions for spectroscopically selected galaxies from the Sloan Digital Sky Survey

Alan Meert,[1]⋆ Vinu Vikram,[1]† and Mariangela Bernardi[1]‡

[1] *Department of Physics and Astronomy, University of Pennsylvania, Philadelphia, PA 19104, USA*

ABSTRACT

We present simulations used to test the two dimensional decompositions of SDSS galaxies utilizing the fitting routine GALFIT and analysis pipeline PyMorph. Analysis showing the bias and scatter of the recovered parameters is presented for multiple combinations of simulated galaxy models and fit types. The simulations show that accurate measurement of single Sérsic models is well constrained when using SDSS-quality data. Two component fits present a less robust image decomposition. Galaxies observed at higher redshift by Hubble are also simulated. We examine the bias created when fitting incorrect models to galaxies. Fitting a two-component Sérsic + Exponential model to what is really just a single Sérsic results in a noisier recovery of the input parameters, but these are not biased; fitting a single Sérsic to what is truly a two-component system results in significant biases. These biases, for total magnitude and halflight radius in particular, should be useful in correcting other automatic fitting routines.

Key words: galaxies: structural parameters – galaxies: fundamental parameters – galaxies: catalogs – methods: numerical – galaxies: evolution

1 INTRODUCTION

Analytical descriptions of photometric galaxy structure are useful data for evaluating models of galaxy dynamics and evolution (e. g., Shankar et al. 2012). Common analytical models include the $r^{1/4}$ and the $r^{1/n}$ models originally presented by de Vaucouleurs (1948) and Sérsic (1963). Model development was driven by observations of elliptical galaxies in the case of de Vacouleurs while Sérsic observed a continuum of early to late-type galaxies. Sérsic attempted to encapsulate the change in profile shape through use of the Sérsic index, n, contained in his model. Subsequent empirical study suggests that bulges and elliptical galaxies are better described by de Vacouleurs profiles or Sérsic profiles with Sérsic index $n \approx 4$. Disks and late-type spirals are best described by exponential profiles, or Sérsic profiles with Sérsic index $n \approx 1$ (Freeman 1970). More recent work has shown that the relationship between Sérsic index and the photometric or kinematic components of a galaxy is more complicated. Following Kent (1985), many analyses simultaneously

fit a second component in order to better accommodate the qualitative differences of bulges and disks in galaxies.

There has been recent work on improving photometric decomposition of galaxies (Simard et al. 2011; Kelvin et al. 2012; Lackner & Gunn 2012) with particular interest on the applicability to evolutionary models. However, different fitting processes continue to produce results which differ qualitatively and quantitatively. Systematics in fitting continue to be of concern, and the reliability of two-component decompositions in cases of low to moderate signal-to-noise are often viewed with some skepticism. In order to quantify the systematics and robustness of the fits presented in Meert, Vikram & Bernardi (2013), hereafter referred to as M2013, we generate simulations of single and two-component galaxies and fit them using the same PyMorph pipeline (Vikram et al. 2010) used for the photometric decompositions presented in M2013. The M2013 catalog has already been used in Bernardi et al. (2012) to study systemmatics in the size-luminosity relation, in Shankar et al. (2012) to study size-evolution of spheroids, and in Huertas-Company et al. (2012) to study the environmental dependence of the mass-size relation of early-type galaxies.

Following several detailed studies which have used sim-

⋆ E-mail: ameert@physics.upenn.edu
† E-mail: vvinuv@gmail.com
‡ E-mail: bernardm@sas.upenn.edu

ulations to test the robustness of different fitting algorithms (e. g., Häussler et al. 2007), the main goal of this paper is to use simulations to test the PyMorph pipeline software. We present more general tests than Häussler et al. (2007). Our simulations are specifically applicable to the SDSS galaxies and are useful for evaluating the decompositions presented in M2013.

A description of the simulation process is presented in section 2. This includes construction of a catalog of realistic galaxy parameters (section 2.1); generating galaxy surface brightness profiles based on these parameters (section 2.2); generating sky and noise (sections 2.3, 2.4); and including seeing effects in the final image. The completed simulations are run through the fitting pipeline and the fits are analyzed in section 3. We examine the recovery of structural parameters in noise-free images (section 3.1) and parameter recovery in realistic observing conditions including both neighboring sources and the effects of incorrect PSF estimation (section 3.2). The effect of changing the fitted cutout size (section 3.3) and the effect of incorrect background estimation (section 3.4) are also examined. PyMorph is further tested by inserting simulated galaxies into real SDSS images to test the dependence on local density (3.5). Finally, we briefly examine the effects of further lowering the signal-to-noise to levels found in the GEMS survey (Häussler et al. 2007), which used the Hubble Telescope Advanced Camera for Surveys (section 3.6). In section 4 we discuss the overall scatter in our fits and the implications of the simulations. Finally, in section 5 we provide concluding remarks.

We generate single component Sérsic galaxy models (hereafter referred to as `Ser`) and two forms of two-component galaxy models: one is a linear combination of de Vacouleurs and an exponential profile (`DevExp`) and and the other replaces the de Vacouleurs with a Sérsic profile (`SerExp`). A good overview of the Sérsic profile used throughout this paper is presented in Graham & Driver (2005). Throughout the paper, a ΛCDM cosmology is assumed with $(h,\Omega_m,\Omega_\Lambda) = (0.7, 0.28, 0.72)$ when necessary.

2   CREATING THE SIMULATIONS

2.1   Selecting the simulation catalog

We create a set of simulated galaxies using fits from the the photometric decompositions presented in M2013. These galaxy parameters represent the r-band image decompositions of a complete sample of the SDSS spectroscopic catalog containing all galaxies with spectroscopic information in SDSS DR7 (Abazajian et al. 2009). Cuts on the surface brightness to ensure completeness and on redshift to prevent contamination of the estimated distance due to peculiar velocity are imposed. A brightest magnitude cut is also applied to remove galaxies that are too close-by and too well resolved to be treated in this simplified manner. The sample and the cuts used are similar to the catalog presented in Simard et al. (2011); see M2013 for more information on the sample of galaxies and the cuts imposed.

The fit parameters of the photometric decompositions were determined using the PyMorph pipeline (Vikram et al. 2010) which uses SExtractor (Bertin & Arnouts 1996) to identify neighboring sources, generates masks, estimates initial parameters and fits galaxies using the GALFIT (Peng

et al. 2002) 2D fitting routine. A number of other non-parametric measurements are also reported.

From the spectroscopic sample, three subsamples of galaxies that are representative of the SDSS spectroscopic catalog and produce physically meaningful photometric decompositions were selected. In order to ensure that the galaxies are representative of the full catalog, we examined the distributions of basic observational parameters of SDSS galaxies (surface brightness, redshift, apparent Petrosian magnitude, Petrosian half-light radius, and absolute magnitude).

Some restrictions on fit parameters are necessary to ensure that outliers are removed from the parameter space used to generate the simulations. Galaxies that do not satisfy these basic cuts are removed to ensure that the parameters used to generate the images are not unphysical. The cuts do not significantly bias our galaxy distribution as is shown in Figure 1. The cuts include:

(i) Any Sérsic components must have Sérsic index less than 8.
(ii) Half-light radius of any Sérsic component must be less than 40 kpc.
(iii) In the two-component fits, the ratio of the bulge halflight radius to disk scale radius should be less than 1, or the galaxy should be bulge dominated (B/T > 0.5).

Conditions (i) and (ii) were chosen to prevent selection of `Ser` models with extended profiles that are likely the result of incorrect sky estimation during the fitting process. Condition (iii) is used to ensure that any disk dominated galaxies have a bulge component that is smaller than the disk.

After enforcing the cuts on the sample of fitted galaxies, 10,000 galaxies for each of the `Ser`, `DevExp`, and `SerExp` samples were selected at random. The fitted parameters of these sample galaxies were used to generate simulated model galaxies used in testing the pipeline.

Figure 1 shows the distributions of surface brightness, redshift, extinction-corrected r-band Petrosian magnitude, r-band Petrosian halflight radius, and absolute magnitude of all SDSS spectroscopic galaxies (in black) and our simulation samples: `Ser` (red), `DevExp` (green), and `SerExp` (blue). The distribution of simulated galaxies reproduces the observed distribution for all three samples for each observational parameter as verified by a KS 2-sample test.

Figure 1 also presents the signal-to-noise (S/N) of the simulation samples as compared to the parent distribution. The S/N of the images is a limiting factor in the fitting process, so care must be taken to ensure that the S/N is not artificially increased in the simulations when compared to true SDSS galaxies. This S/N is calculated using the r-band Petrosian magnitude and r-band Petrosian halflight radius. Petrosian quantities are used to make a fairer comparison among all the samples. Because the Petrosian quantities are non-parametric, they avoid the complications that arise in assessing the possible biases introduced during fitting. Any differences in S/N are not large enough to significantly bias the distributions as verified by the KS 2-sample test. Therefore, we conclude that our samples are fair representations of the underlying distribution of SDSS spectroscopic galaxies.

An unbiased selection in the previously mentioned parameters is not sufficient to guarantee fair sampling of the S/N with respect to magnitude, nor does it prevent ficti-
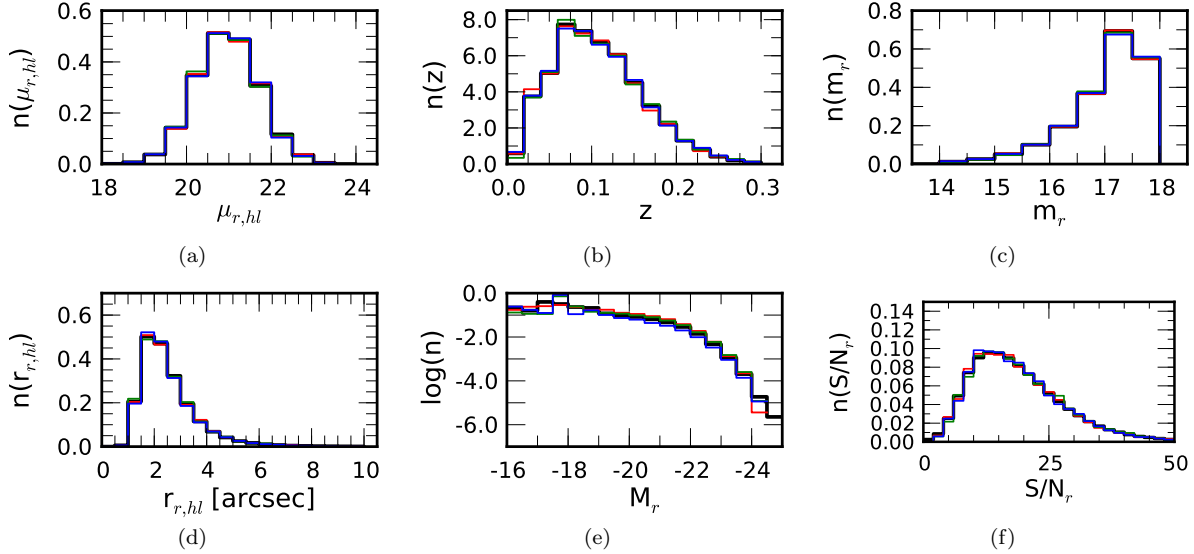
Figure 1. (a) The surface brightness distribution, **(b)** redshift distribution, **(c)** extinction-corrected r-band Petrosian magnitude, **(d)** r-band Petrosian halflight radius, **(e)** V_{max}-weighted luminosity function, and **(f)** signal-to-noise distribution of the simulated sample of galaxies drawn from the SDSS spectroscopic galaxy sample of DR7. The distribution of all SDSS spectroscopic galaxies is shown in black. Distributions of the `Ser`, `DevExp`, and `SerExp` simulations are shown in red, green, and blue, respectively. Bin counts are normalized to integrate to 1. The distributions of the simulated galaxies are representative of the full sample fitted in M2013 and are appropriate to compare to the SDSS spectroscopic sample as verified by a Kolmogorov-Smirnov 2-sample test. The signal-to-noise (S/N) will be discussed further in section 2.4. In calculating this S/N, we use the measurement of sky provided by the PyMorph pipeline rather than SDSS to identify and separate target counts from sky counts. PyMorph sky estimation is shown to be more accurate than the SDSS estimation provided in the DR7 catalog.

tious correlations among multiple fit parameters. In fact, correlations among fit parameters are to be expected if the PyMorph pipeline is robustly measuring properties of the target galaxies (there are many obvious correlations that exist among parameters, as evidenced by the numerous scaling relations that currently exist). However, it is difficult, and largely unnecessary, to examine every possible relationship thereby ensuring that all correlations are true reflections of the underlying data.

Two important relationships are the halflight radius as a function of apparent magnitude and the S/N as a function of the apparent magnitude. The two relationships are necessary to ensure the appropriateness of the simulation because systematic differences in radius will lead to systematic variation in the S/N of the sample. Scatter in the recovered fitting parameters as a function of magnitude is particularly useful, since it is relatively easy to estimate total magnitude on image data. Therefore, the S/N as a function of apparent magnitude should appropriately reflect that of the parent sample from SDSS.

Figure 2 presents the halflight radius versus apparent magnitude, and Figure 3 presents the S/N versus apparent magnitude. The simulated samples are shown in red, green, and blue corresponding to the `Ser`, `DevExp`, and `SerExp` models. The underlying SDSS parent distribution is shown in black. Indeed, Figure 2 shows that the `Ser` and `SerExp` models are in close agreement with the full SDSS sample. The `SerExp` sample has smaller radii (about 10% smaller) in the brightest magnitude bin ($14.0 < m_{tot,r} < 14.5$). The `Ser` model radii agree across the magnitude range. However, the S/N agrees with the full SDSS sample, or is slightly below that of SDSS. The lower signal-to-noise, although not
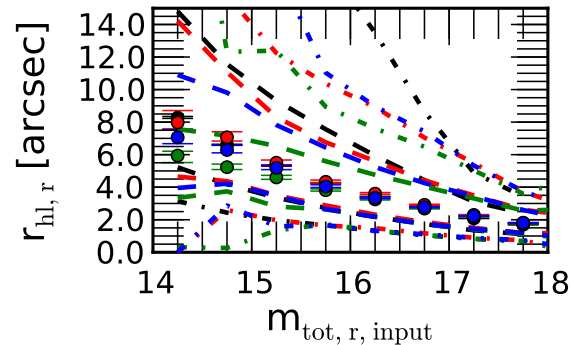

Figure 2. The distribution of galaxy radii as a function of apparent magnitude for the parent SDSS sample in black, the `Ser` model in red, the `DevExp` model in green, and the `SerExp` model in blue. The median in each bin is shown with corresponding contours showing the extent of the middle 68% of data (dashed lines) and middle 95% of the data (dot-dashed lines). At brighter magnitudes, the `DevExp` model begins to diverge from the original sample toward smaller radi. The `SerExp` model is in closer agreement across the entire magnitude range.

exactly that of SDSS will not bias the tests toward better results, so we deem these samples acceptable for testing. The `DevExp` model tends to smaller radii and higher S/N at brighter magnitude. The `DevExp` model was also analyzed, however the results are not discussed in this paper. They can be found in Meert et al. (2013).

Testing the accuracy of the PyMorph fitting routine does not necessarily require an unbiased parameter distri-
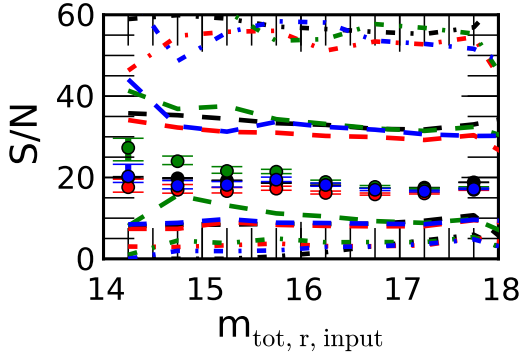
Figure 3. The distribution of galaxy S/N as a function of apparent magnitude is presented in the same format as Figure 2. At brighter magnitudes, the `DevExp` model begins to diverge from the original sample toward higher S/N. The `SerExp` and `Ser` models are in closer agreement across the entire magnitude range.

bution. In reality, all that is required is a sample with sufficient coverage of the parameter space represented by the data. The simulations use smooth profiles, simplifications of the true galaxies that are observed in SDSS. Examination of the results of fitting these simplified models and comparison to fits of true observed galaxies can potentially yield useful information regarding galaxy structure. In Bernardi et al. (2012), the simulations are used together with the decompositions of the SDSS spectroscopic sample to characterize the scatter in the size-luminosity relation as well as examine possible biases. In order to make these comparisons, an unbiased sample is required. The distributions shown in Figure 1 show that the simulations are appropriate to use for this purpose.

2.2   Generating the images

We generate the two-dimensional normalized photon distributions from the one-dimensional Sérsic profiles and the one-dimensional exponential profiles of each bulge and disk component. Disk components are only simulated where required, as is the case for two-component fits. When multiple components are to be simulated, each component's normalized photon distribution is generated separately and combined prior to generating the simulated exposure.

Two-dimensional galaxy profiles are treated as azimuthally symmetric one-dimensional galaxy light profiles that are deformed according to an observed ellipticity. The galaxy profiles are generated using the structural parameters generated from photometric decompositions as described in the previous section. Single component galaxy profiles and the bulges of two component galaxies are generated according to the Sérsic profile

$$I(r) = I_e \exp\left(-b_n \left[\left(\frac{r}{R_e}\right)^{\frac{1}{n}} - 1\right]\right) \tag{1}$$

$$b_n = 1.9992n - 0.3271$$

where Sérsic index (n), half-light radius (R_e), and surface brightness at $R_e(I_e)$ are selected simultaneously from the catalog described in the previous section.

For the `DevExp` and `SerExp` cases, an exponential disk

(the formula above, with $n = 1$) is added to the Sérsic component to model the disk component of the galaxies. This model requires input parameters scale radius (R_d) and central surface brightness (I_d). The disk is modeled using

$$I_{Exp}(r) = I_d \exp\left(\frac{-r}{R_d}\right). \tag{2}$$

The disk profile can be recast as equation (1) by noting that the exponential profile is a special case of the general Sérsic profile. The equivalence is true when

$$I_d = I_e \exp b_n, \quad R_e = (b_n)^n R_d, \quad \text{and} \quad n = 1. \tag{3}$$

The one-dimensional profiles are made into two dimensional profiles by assuming a uniform distribution in angle θ.

At this point, there is no explicit dependence in the profiles on the position angle, ϕ, of the components. Therefore, we begin by treating each component as having the major axis coincident with the x-axis. For example, a photon with $\theta = 0$ will fall on the semi-major axis of the galaxy while a photon with $\theta = \pi/2$ will fall on the semi-minor axis.

The continuous image in (r, θ) space is then transformed into (x, y) space in the plane of the sky using the axis ratio (b/a) of the respective component according to the equations

$$x = (b/a)^{1/2} \ r \cos\theta$$
$$y = (b/a)^{-1/2} \ r \sin\theta \ . \tag{4}$$

At this point, the component major axis is still coincident with the positive x axis. To rotate by the true position angle of the component (ϕ_d for the disk or ϕ_b for the bulge), we use the standard rotation matrix

$$R = \left(\begin{array}{cc} \cos\phi & -\sin\phi \\ \sin\phi & \cos\phi \end{array}\right) \tag{5}$$

where $\phi = \phi_b$ or ϕ_d depending on which component is currently being simulated (bulge or disk component, respectively).

For true bulges, the axis ratio defines an intrinsic ellipticity of the bulge. More exactly, this ellipticity is believed to be a two-dimensional projection of an intrinsically elliptical object. On the other hand, we treat the exponential portions of galaxy profiles as an infinitesimally thin disk. Rotationally supported thin disk components are thought to be intrinsically round, and so their ellipticity is not interpreted as a true ellipticity but rather a projection effect due to the line of sight used to view the disk. For this reason, the disk ellipticity is often expressed as an inclination, ψ_d, where

$$\psi_d = \cos^{-1}(b/a) \tag{6}$$

so that $b/a = 1$ implies $\psi_d = 0$ (the observer is viewing the disk face-on) and $b/a = 0$ implies $\psi_d = \pi/2$ (the observer is viewing the disk edge-on).

After rotation, the continuous probability distribution represented by the two-dimensional light profile can be integrated over pixel areas to define a pixellized probability distribution. The details of this integration are mainly unimportant. However, the simulation must take careful account of the integration in the central pixels, where the profile can vary greatly over a single pixel. Various oversampling methods have been devised to properly correct this common problem (e. g., Peng et al. 2002; Häussler et al. 2007).
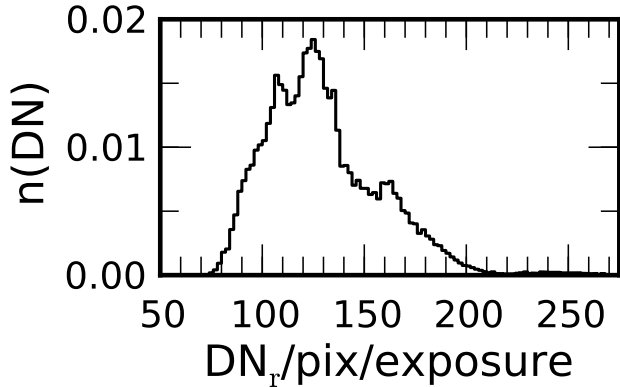
Figure 4. The distribution of sky values for data in the SDSS CASJOBS catalog. These data are drawn from the `sky_r` CASJOBS parameter and are converted into counts (DN) per pixel per standard SDSS image exposure of 54 seconds. We use this distribution to determine the sky value used in our simulations. As an approximation, we use the mean value of 130 counts/pixel/exposure.

The simulations in this paper have been tested to ensure that the pixel-by-pixel integration is accurate to $\approx 3\%$ of the corresponding Poisson noise in a given pixel. Therefore, we treat the simulations as exact calculations of the galaxy photon distributions.

After generating image, the galaxy is numerically convolved with a PSF extracted from SDSS DR7 data using `read_PSF` program distributed by SDSS[1].

2.3 Creating the background

Two hundred background images, each equal in size to an SDSS fpC image, are also simulated for testing purposes. These images contain constant background and a randomly selected field of galaxies taken from an SDSS fpC image. The SDSS catalog provides rudimentary photometric decompositions of each star and galaxy. Galaxies are fit with an exponential disk and a de Vacouleurs ($n = 4$) bulge independently. The best fit is reported as a linear combination of the two fits using the `fracdev` parameter to express the ratio of the de Vacouleurs model to the total light in the galaxy.

For the simulated background used in this paper, each galaxy is generated using the combined profile of the two fits. The de Vacouleurs bulge and exponential disk component are separately simulated according to the magnitude, radius, ellipticity, and position angle reported in SDSS. Each component is simulated using the method described in section 2.2. The background galaxy is constructed by adding the two components using the `fracdev` parameter. The galaxy is then inserted into the fpC image. Any foreground stars are also simulated as point sources and inserted into the image.

For the background sky counts in the image, we use the mean sky of all SDSS observations as given in the SDSS `photoobj` table by the `sky_r` parameter. The distribution of the sky flux is plotted in Figure 4 in units of counts (or DN) per pixel per exposure. The median and mean values

for a 54 second SDSS exposure are ≈ 125 and ≈ 130 counts per pixel, respectively. We use the mean value of 130 counts per pixel as the background in our simulations. This sky background is applied to the entire chip as a constant background; no gradient is simulated across the image. Background gradients should be approximately constant across a single galaxy. This assumption is verified by inserting the simulated galaxies into real SDSS fpC images near known clusters, where the sky contribution should be high and gradients more likely. In section 3.5 we show that there is little change in the behavior of the fits in these types of environments.

Previous work has improved the measurements of sky background (see Blanton et al. 2011). However, these corrections are largely focused on areas of large, bright galaxies or on making the sky subtraction stable for purposes of tiling fpC images together. Since we are only focused on maintaining the proper S/N for our simulations, the sky levels provided in the SDSS database are sufficient, provided that they maintain the correct S/N. We discuss the S/N distribution of our simulations and the original SDSS galaxy sample in section 2.4 below.

Diffraction spikes and other image artifacts are not simulated. However, the SDSS `photo` pipeline often misidentifies additional phantom sources along any observed diffraction spike. These sources may be modeled in our background, and so these effects may, in fact, be approximately modeled, albeit unintentionally. It is reasonable to expect that the diffraction effects should not have a large effect on the fitting process, as their elongated straight structure does not mimic galaxy structure. The dominant effect produced by the bright stars in the field is bias in the background estimation in the nearby neighborhood of a star.

After simulation of the background images, and prior to adding noise, each background image is convolved with a random SDSS PSF selected from original fpC image upon which the individual image is based.

2.4 Noise

After generating a target galaxy and inserting it into a background, Poisson noise is added using the average inverse gain of an SDSS image ($4.7\ e^-/\mathrm{DN}$) and the average contribution of the dark current and read noise, referred to as the "dark variance," ($1.17\ \mathrm{DN}^2$), to determine the standard deviation for each pixel. Specifically,

$$F_{i,j} \equiv I_{i,j} + \mathrm{bkrd}_{i,j} \qquad (7)$$

is the total flux in pixel (i, j) (i.e., , the sum of the source and background fluxes in the pixel), and

$$\sigma_{i,j} = \sqrt{\frac{F_{i,j}}{\mathrm{gain}} + \mathrm{dark\ variance}} \qquad (8)$$

so

$$\left(\frac{\mathrm{S}}{\mathrm{N}}\right)_{i,j} \equiv \frac{I_{i,j}}{\sigma_{i,j}}, \qquad (9)$$

for a single pixel.

Since the fitting pipeline is dependent on the S/N, it is essential that the simulated S/N is comparable to SDSS. The distribution of the average S/N per pixel within the halflight radius for the simulations and the original galaxies

---

[1] `read_PSF` is part of the `readAtlasImages-v5_4_11` package available at `http://www.sdss.org/dr7/products/images/read_psf.html`

is plotted in Figure 1(f). The S/N distribution of simulations and the SDSS spectroscopic galaxies agree as verified by a KS 2-sample test, therefore the simulations appropriately approximate the S/N of SDSS galaxies contained in M2013.

2.5 Final processing for fitting

After constructing the images, we generate an image of the $\sigma_{i,j}$ values according to equation 8. This image is supplied along with the input image to the pipeline in order to calculate the χ^2 value for the fit.

Figure 5 shows some examples of simulated galaxies throughout the simulation process. This includes the noiseless simulated galaxy, the noiseless simulated background, the composite image of galaxy and background, and the composite image after adding Poisson noise with $\sigma_{i,j}$ defined in equation 8. The final image size used for fitting is 20 times the Petrosian r-band halflight radius. A discussion of this choice of stamp size is presented in section 3.3.

3 TESTING PYMORPH IMAGE DECOMPOSITIONS

PyMorph was used to fit the simulated galaxies described above in section 2. In order to describe and quantify the amount of bias and scatter in the PyMorph image decomposition pipeline when applied to SDSS simulations, several tests of increasing complexity were performed. The primary focus is on the systematics of the pipeline. A better understanding of these systematic effects is useful in interpreting the data presented in M2013.

3.1 Noiseless images

As an initial test, the pipeline is applied to galaxies with no noise and no neighboring sources or background counts. This produces the minimum scatter in the data, serves to verify that our simulations are correct, and shows that PyMorph is properly functioning.

The total apparent magnitude, halflight radius, and additional fit parameters recovered by fitting the noiseless images of the Ser and SerExp models are presented in Figures 6(a), 7(a), 8(a), 9(a), and 10(a). The plots show the difference in simulated and fitted values (fitted value - input value) versus the input value. The greyscale shows the density of points in each plane with red points showing the median value. Blue dashed lines show the regions which contain 68% of the objects.

Figures 6(a) and 9(a) show the corresponding fit is well constrained (Ser fit with Ser, and SerExp with SerExp) although the scatter increases somewhat for the components of the SerExp fit (see Figure 10(a)). This is most true as the component becomes dim (bulge/disk magnitude approaches 18) where S/N for the individual component drops more rapidly. The magnitude and halflight radius are also well constrained when a Ser galaxy is fit with a SerExp profile (Figure 7(a)). However, a SerExp galaxy fit with a Ser profile produces large biases in the magnitude and halflight radius (Figure 8(a)).

The total magnitude and halflight radius are well constrained ($\sigma_{\text{total mag}} \approx 0.01$ mag and $\sigma_{\text{radius}} \approx 0.1$ arcsec)

in cases where the correct model is applied to the simulated galaxy (i.e., Ser galaxy fit with a Ser model). This is not necessarily the case when the wrong model is applied (i.e., SerExp galaxy fit with a Ser model). It is obvious that a single-component galaxy cannot properly model a two-component galaxy in general, and therefore, we would expect significant problems in attempting to fit a single component profile to a two-component galaxy. Nevertheless, this type of fit is often performed on real data when it is believed that the resolution and S/N are such that it is unlikely to recover a robust two-component fit. An important observation is that the SerExp fit provides the most stable estimate of the halflight radius and total magnitude regardless of the true simulated galaxy model (Ser, DevExp, or SerExp). The additional freedom in the SerExp model and the fact that the Ser and DevExp models are special cases of the SerExp model would lead us to expect this result.

One noticeable systematic in the pipeline, one that has proven difficult to eliminate, is the underestimate of Sérsic index at larger Sérsic indexes. At Sérsic indexes of $n \approx 4$, we underestimate the Sérsic index by less than 1%. However, this underestimate increases in the later tests.

Since no Poisson noise is added to these images, the effective S/N is much larger than the S/N of an SDSS image that the PyMorph pipeline is expected to analyze. The scatter apparent in these fits is then a combination noise associated with the use of the PyMorph routine (as well as the GALFIT routine used by PyMorph) and any parameter degeneracies inherent in the models.

GALFIT uses the Levenberg-Marquardt minimization method (Press et al. 1992) to find the minimum of the χ^2 distribution of the fit. The Levenberg-Marquardt method is not a global search algorithm but rather follows the steepest decent to a local minimum. As the parameter space becomes more complicated, GALFIT has more trouble accurately recovering parameters. Adding components to the fit (i.e., going from a one-component to two-component fit or going from a fixed Sérsic index component to one with a free Sérsic index) will not only complicate the χ^2 surface, making convergence less likely, but may introduce true degeneracies in the parameter space.

For instance, the SerExp fit of a galaxy of very late type often suffers from over-fitting. The bulge component will tend to fit the disk of the galaxy as a second disk component with $n \approx 1$. This is obviously an unintended solution to the fitting, but one that is equally valid from a χ^2 perspective. In practice, it is difficult to prevent this type of convergence without artificially constraining the fitting routine. Such constraints are generally discouraged and can lead to other negative effects including convergence to a non-optimal solution. The best solution to the parameter degeneracy is close examination of any two-component fits in cases where $n \approx 1$, or B/T ≈ 0 or $1-$B/T≈ 0.

3.2 The effects of background, neighbor sources, and incorrect PSF extraction

When analyzing real data, it is not possible to extract the PSF of the target galaxy to arbitrary accuracy. Interpolation is required and generally performed on a network of the nearest stars to the target galaxy. We test this effect through
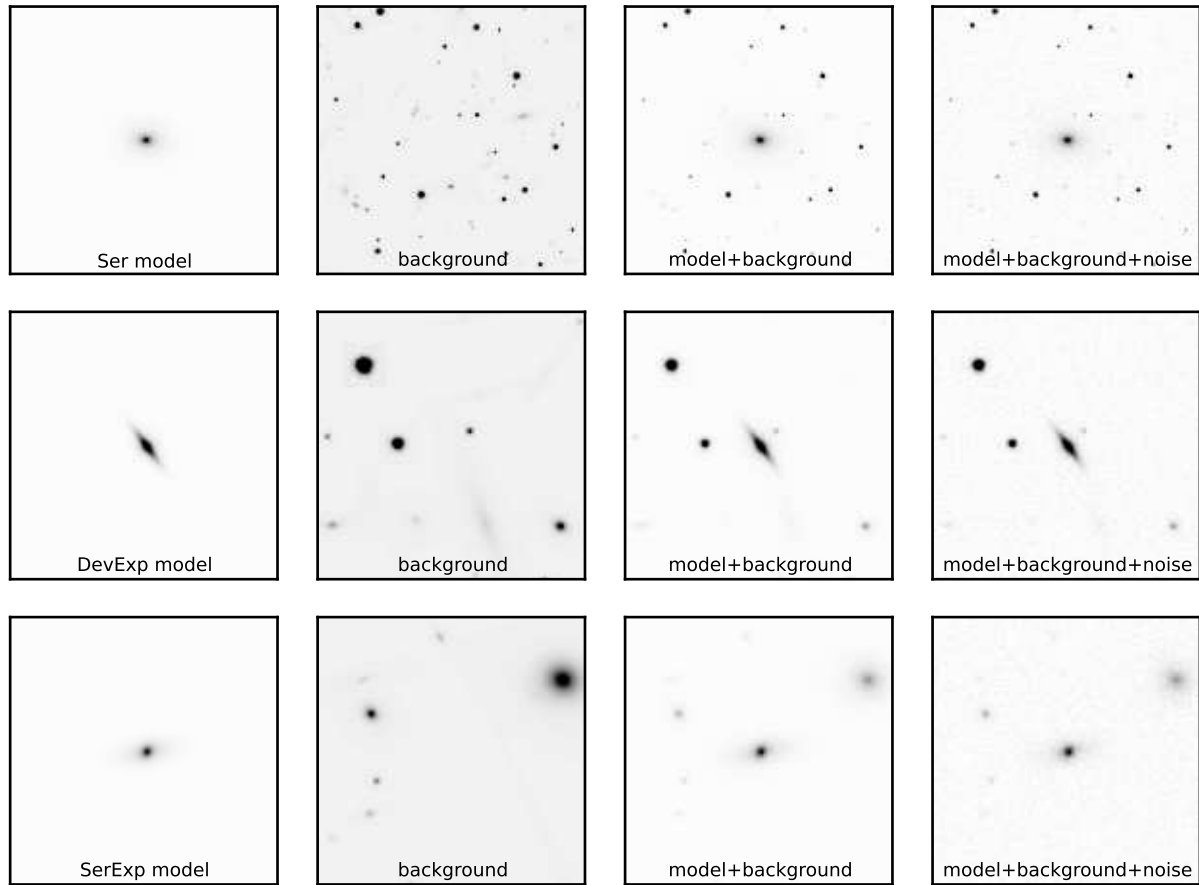
Figure 5. Examples of simulated galaxies and background shown before and after adding Poisson noise. Top, middle and bottom rows show randomly selected sample `Ser`, `DevExp`, and `SerExp` profiles, respectively. From left to right, the columns show the simulated galaxy, simulated background, background+galaxy, and final image with noise.

extraction of a neighboring PSF to be used during fitting in place of the PSF used to generate the image.

The neighbor PSF used in fitting is randomly selected from a location within a 200 pixel box surrounding the source. This provides approximately even sampling of distances from nearly 0 to about 170 pixels in separation from the source which corresponds to a separation of ≈ 0 to ≈ 67.32 arcseconds between the target galaxy and the location used for PSF extraction. This inserts some PSF error into the process of fitting as would be expected in the case of real data. However, it also retains the similarity between the PSF used for simulation and the PSF used for fitting. A strong similarity between the two would be expected since the PSF generally will not vary greatly over the area of a single fpC image.

The PSF effect is applied to target galaxies randomly inserted into the simulated fpC images described in section 2.3. The simulated fpC images contain sky as well as neighboring sources. These fits are the closest simulation to actual observing conditions that we have analyzed. Therefore the fits and the resulting measures of scatter and bias are adopted as our fiducial estimates of scatter and bias when using the pipeline.

Figures 6(b), 7(b), 8(b), 9(b), and 10(b) show that

we recover the input values with marginal scatter. The total magnitude and halflight radius remain well constrained ($\sigma_{\mathrm{totalmag}} \approx 0.05$ mag and $\sigma_{\mathrm{radius}} \approx 0.25$ arcsec) in cases where the correct model is fit to the simulated galaxy. However, this scatter becomes much larger when the wrong model is fit. The underestimate of the Sérsic index, particularly at large values, persists.

Further examination of the two component fits show that the pipeline has difficulty extracting dim components (bulge or disk magnitude dimmer than ≈ 18). In these ranges, the components are observed at lower S/N and the pipeline looses sensitivity to the model parameters. The `SerExp` fit shows an underestimate of Sérsic index, which is even stronger than in the single component case, and an underestimate of bulge radius. However, the disk parameters remain unbiased with an increase in scatter of the model parameters. Most likely, this stability is the result of the fixed Sérsic index of the bulge ($n = 1$) which fixes the shape of the disk light profile.

In general, the `SerExp` fits are problematic and require much care when analyzing individual components. However, as we have already shown, total magnitude and halflight radius are still tightly constrained.
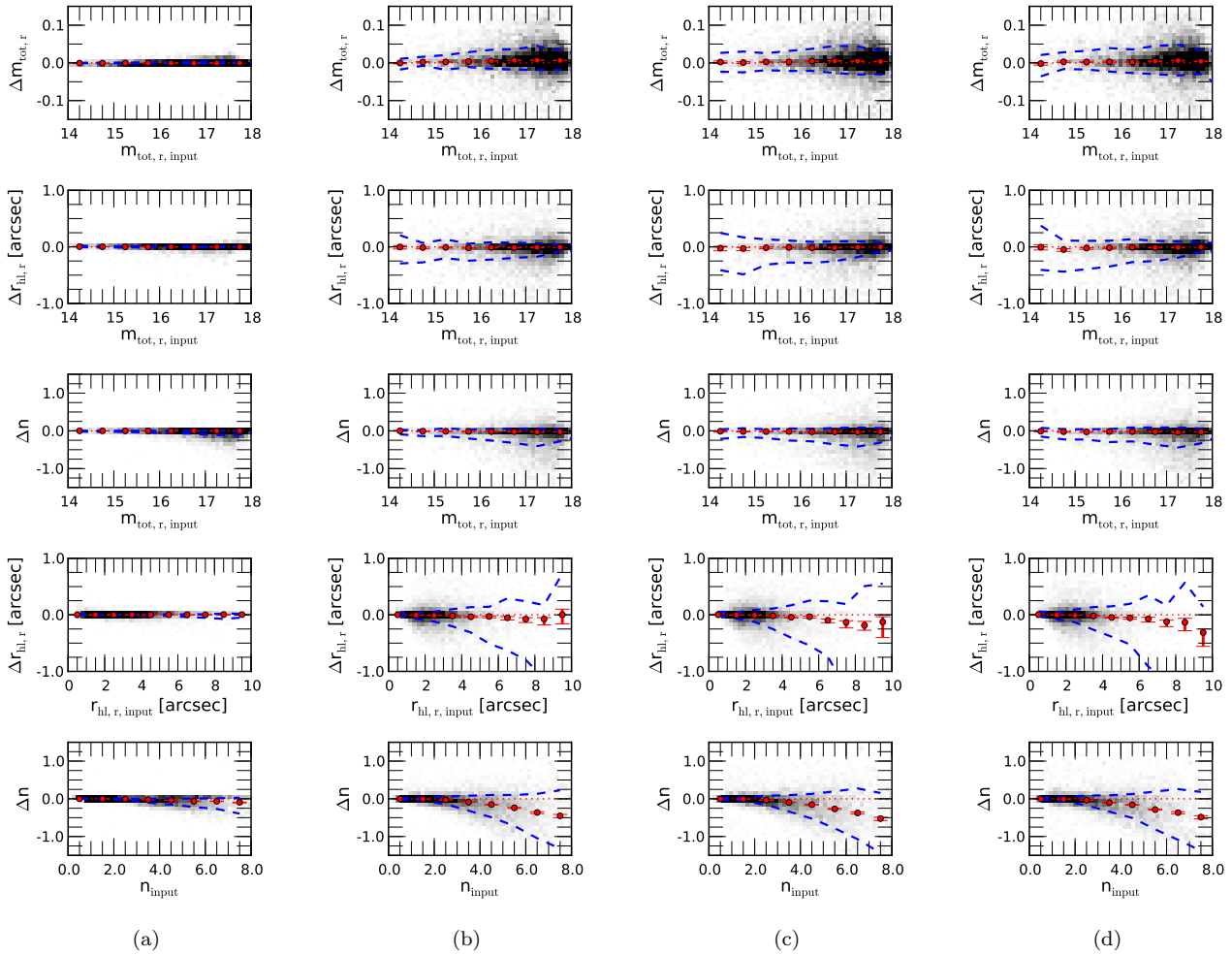
Table 1 summarizes the bias and scatter in the fits; they

Figure 6. The simulated and recovered apparent magnitude, halflight radius, and Sérsic index for a `Ser` galaxy fit with a `Ser` model in four cases: **(a)** the image prior to adding Poisson noise, **(b)** our fiducial case containing simulated sky and neighboring sources, **(c)** the simulated galaxies inserted into real SDSS fpC images, and **(d)** the simulated galaxies inserted into real SDSS fpC images near clusters. Over-plotted are the bias (red points) in the fitted values. All plots show the 68% (dashed line) scatter in blue. The density of points is plotted in gray-scale. The Sérsic index shows increasing underestimate up to ≈ 0.5 (or $\approx 8\%$) at the largest Sérsic indexes.

exhibit trends with both the input value of the parameter and the input magnitude of the galaxy. This behavior is not properly encapsulated in the overall measure of bias, so these values are useful only as an example of the relative scale of bias and scatter for each parameter.

Errors can be correlated across many fit parameters, so we also calculate a correlation matrix for the parameter errors. Figure 11 shows an example of the correlation matrix for the simulated `SerExp` galaxies fit with a `SerExp` model. We see the expected strong correlations between bulge-to-light ratio and the bulge and disk magnitudes as well as the correlation among the radii of the bulge component with the Sérsic index. While the correlation matrix suggests that there is little correlation between sky estimation error and the fitted parameters, we will show later that there is indeed a strong correlation in model errors with sky estimation error.

3.3 Effect of cutout size

We select postage stamp cutouts for use in fitting. It is important to select a cutout size that does not significantly bias the fits produced by PyMorph. The most important consideration is to provide enough sky pixels to allow the PyMorph program to properly determine the sky level in the images. Reducing cutout size may cause overestimation of background and corresponding errors in the other fit parameters. However, we use the PyMorph pipeline and GALFIT to fit a constant background to the galaxy image. Since a larger image could make sky gradients more significant, this could bias the fits when a larger cutout is used. We seek to minimize error when estimating the sky level without introducing a gradient term and further complicating the fitting process.

To test for optimal cutout size, we fit simulated galaxies with cutout sizes between 10 and 25 Petrosian half-light radii. We plot the average difference between simulated and measured fit parameters below. In Figure 12 we present the error and 1-σ scatter in the error on the total magnitude,
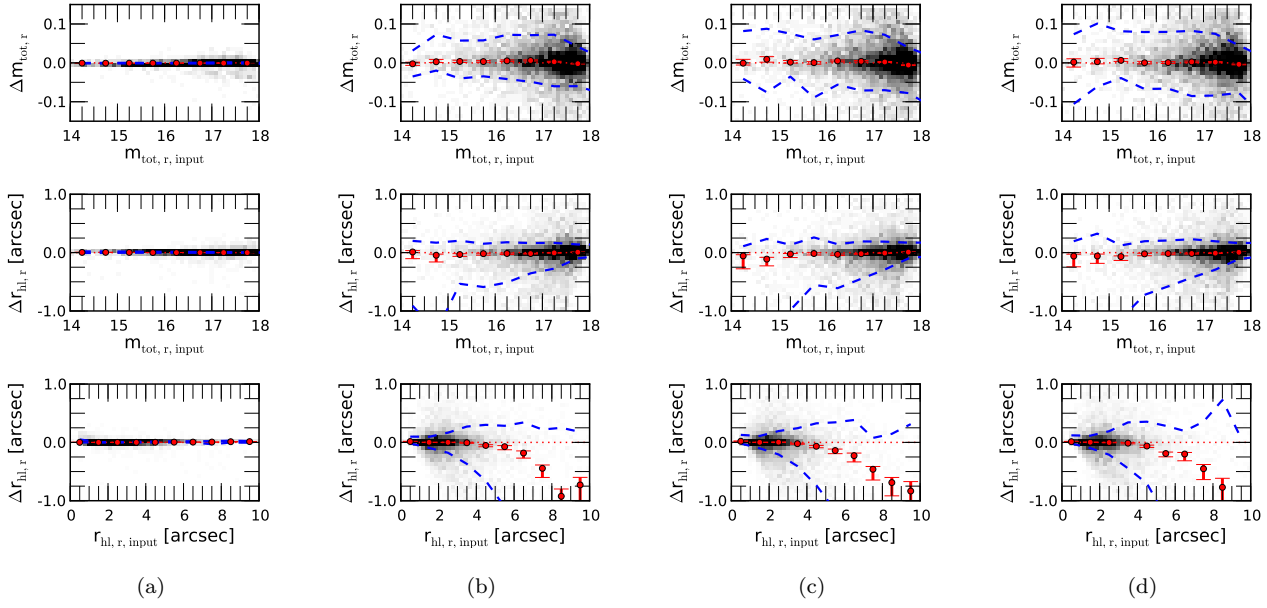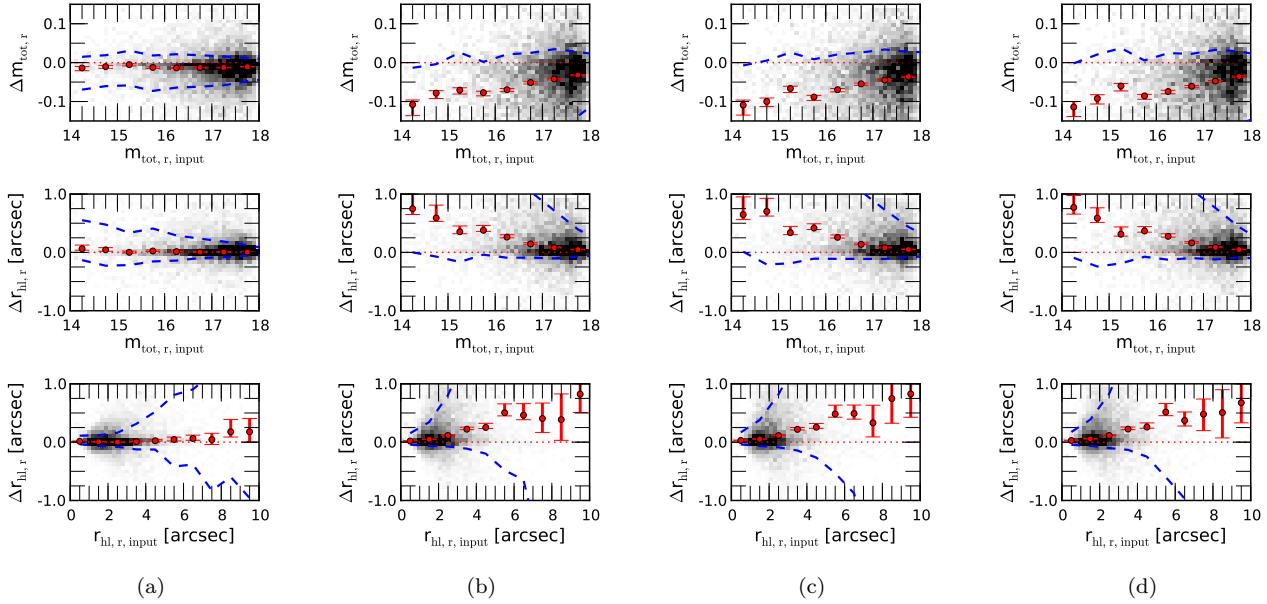
Figure 7. The simulated and recovered apparent magnitude and halflight radius for a `Ser` galaxy fit with a `SerExp` model in four cases: **(a)** the image prior to adding Poisson noise, **(b)** our fiducial case containing simulated sky and neighboring sources, **(c)** the simulated galaxies inserted into real SDSS fpC images, and **(d)** the simulated galaxies inserted into real SDSS fpC images near clusters. Over-plotted are the bias (red points) in the fitted values. All plots show the 68% (dashed line) scatter in blue. The density of points is plotted in gray-scale.

Figure 8. The simulated and recovered apparent magnitude and halflight radius for a `SerExp` galaxy fit with a `Ser` model in four cases: **(a)** the image prior to adding Poisson noise, **(b)** our fiducial case containing simulated sky and neighboring sources, **(c)** the simulated galaxies inserted into real SDSS fpC images, and **(d)** the simulated galaxies inserted into real SDSS fpC images near clusters. Over-plotted are the bias (red points) in the fitted values. All plots show the 68% (dashed line) scatter in blue. The density of points is plotted in gray-scale. The inability of the `Ser` profile to accurately model a `SerExp` galaxy is clearly evident. Errors in magnitude and halflight radius are correlated and the error in radius is largely driven by errors in the largest, brightest objects. However, systematic errors occur even at the dimmer magnitudes. `Ser` fits tend toward recovering larger, brighter objects when applied to a true two component galaxy.
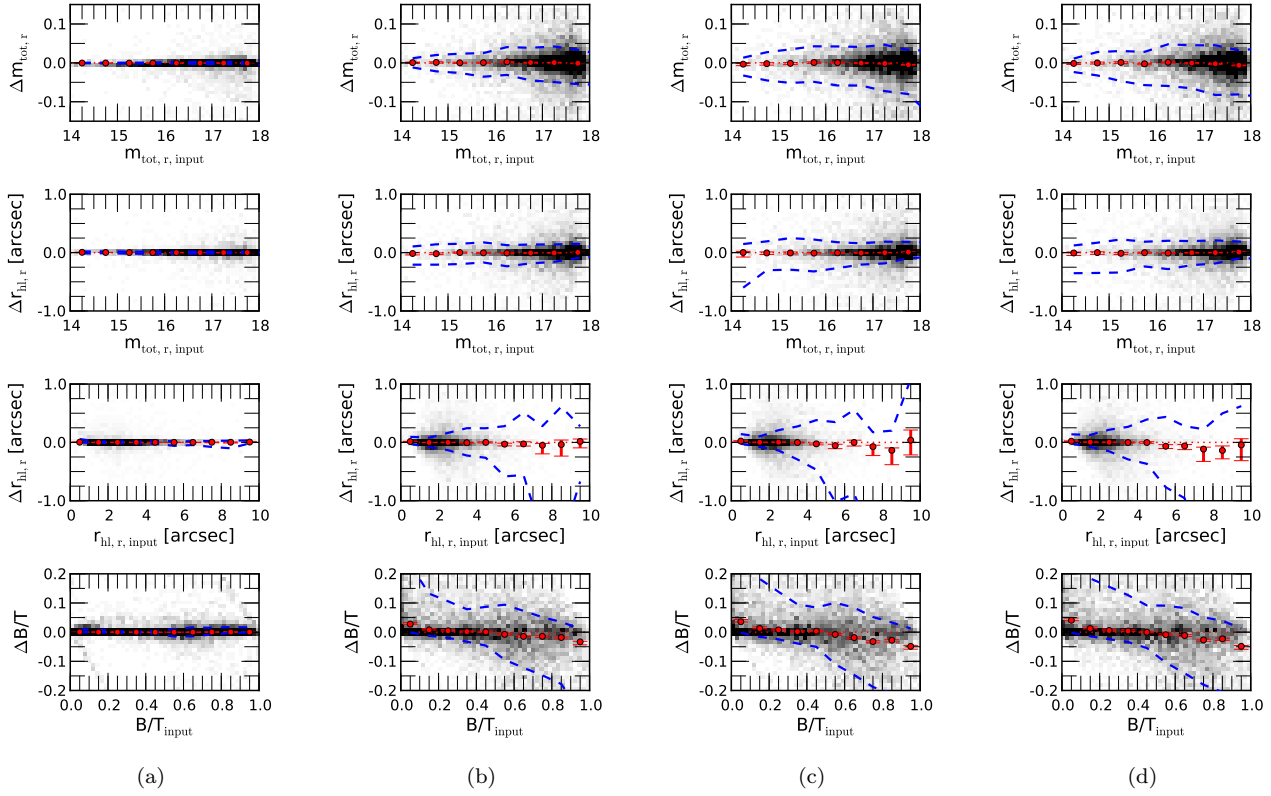
Figure 9. The simulated and recovered apparent magnitude, halflight radius, and bulge-to-total light ratio for a `SerExp` galaxy fit with a `SerExp` model in four cases: **(a)** the image prior to adding Poisson noise, **(b)** our fiducial case containing simulated sky and neighboring sources, **(c)** the simulated galaxies inserted into real SDSS fpC images, and **(d)** the simulated galaxies inserted into real SDSS fpC images near clusters. Over-plotted are the bias (red points) in the fitted values. All plots show the 68% (dashed line) scatter in blue. The density of points is plotted in gray-scale. The apparent trend in B/T from overestimation at lower B/T values to underestimation at higher B/T values is largely due to the boundaries on the parameter space forcing the scatter to be asymmetric (e.g., a galaxy with true B/T= 1 cannot be estimated to have B/T> 1).

Simulated model	Parameter	fitted model			
		Ser		SerExp	
		bias	1-σ	bias	1-σ
Ser	m_{tot} [mag]	0.00 ± 0.09	$[-0.02, 0.02]$	-0.02 ± 0.18	$[-0.11, 0.02]$
	r_{hl} [arcsec]	-0.01 ± 0.68	$[-0.14, 0.01]$	0.11 ± 1.53	$[-0.11, 0.04]$
	sky [%]	-0.05 ± 0.14	$[-0.11, -0.05]$	-0.05 ± 0.14	$[-0.11, -0.05]$
	Sérsic Index	-0.08 ± 0.57	$[-0.44, 0.01]$	–	–
SerExp	m_{tot} [mag]	-0.07 ± 0.18	$[-0.22, -0.01]$	-0.02 ± 0.15	$[-0.09, 0.01]$
	r_{hl} [arcsec]	0.49 ± 1.86	$[-0.02, 0.30]$	0.07 ± 1.17	$[-0.07, 0.04]$
	sky [%]	-0.08 ± 0.15	$[-0.16, -0.07]$	-0.06 ± 0.13	$[-0.11, -0.05]$
	B/T	–	–	0.00 ± 0.15	$[-0.07, 0.03]$
	m_{bulge} [mag]	–	–	-0.14 ± 0.71	$[-0.73, 0.06]$
	m_{disk} [mag]	–	–	-0.04 ± 0.50	$[-0.41, 0.05]$
	r_{bulge} [arcsec]	–	–	0.08 ± 0.97	$[-0.27, 0.11]$
	r_{disk} [arcsec]	–	–	0.07 ± 0.82	$[-0.14, 0.08]$
	Sérsic Index	–	–	0.06 ± 1.98	$[-0.90, 0.14]$

Table 1. The bias and scatter of the fitted parameters of the simulated images with background and PSF effects. These values are provided for illustrative purposes only. There is much underlying structure in the errors when compared to their respective input values or the magnitude of the component.
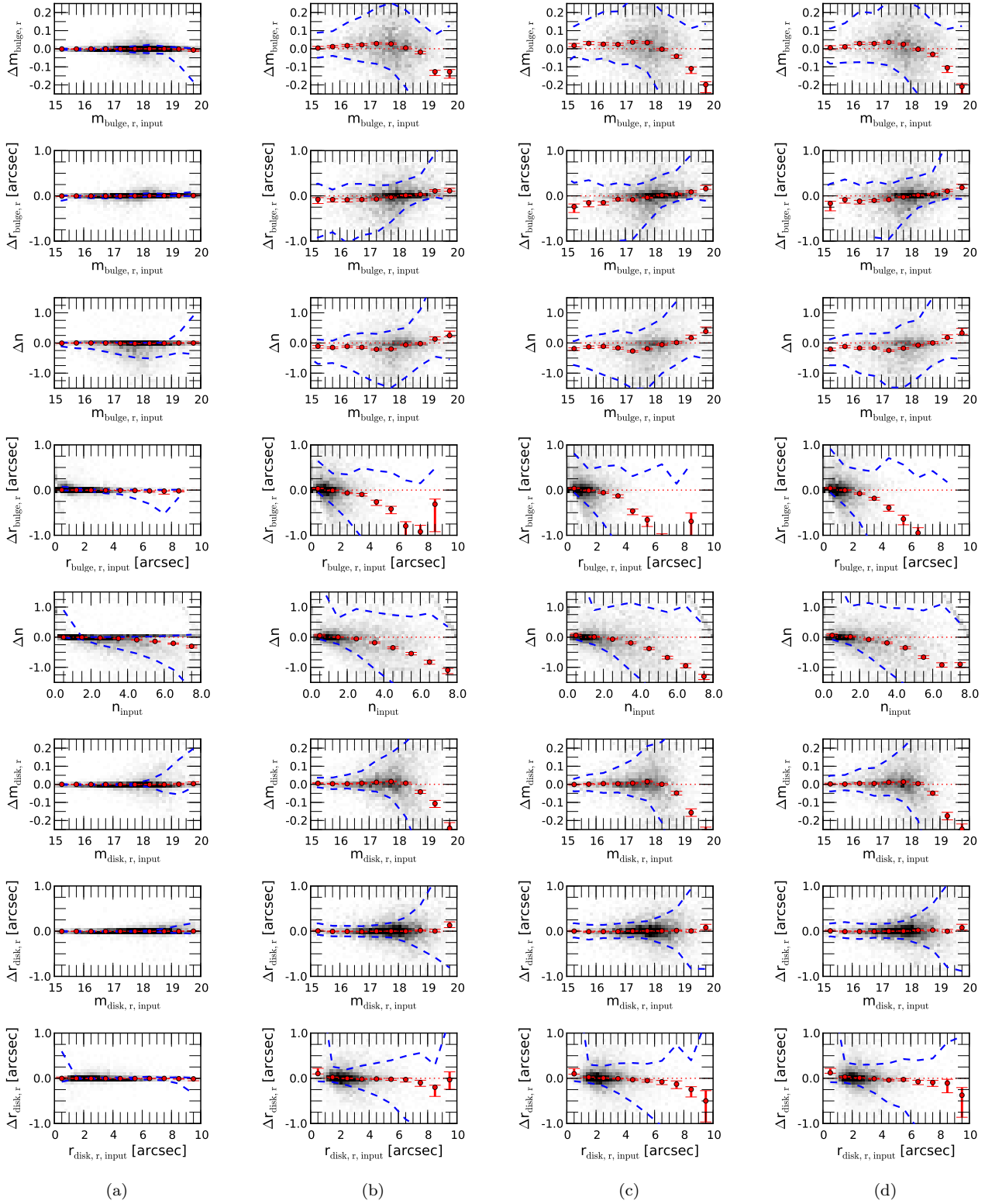
Figure 10. The simulated and recovered component parameters for a `SerExp` galaxy fit with a `SerExp` model in four cases: **(a)** the image prior to adding Poisson noise, **(b)** our fiducial case containing simulated sky and neighboring sources, **(c)** the simulated galaxies inserted into real SDSS fpC images, and **(d)** the simulated galaxies inserted into real SDSS fpC images near clusters. Over-plotted are the bias (red points) in the fitted values. All plots show the 68% (dashed line) scatter in blue. The density of points is plotted in gray-scale.
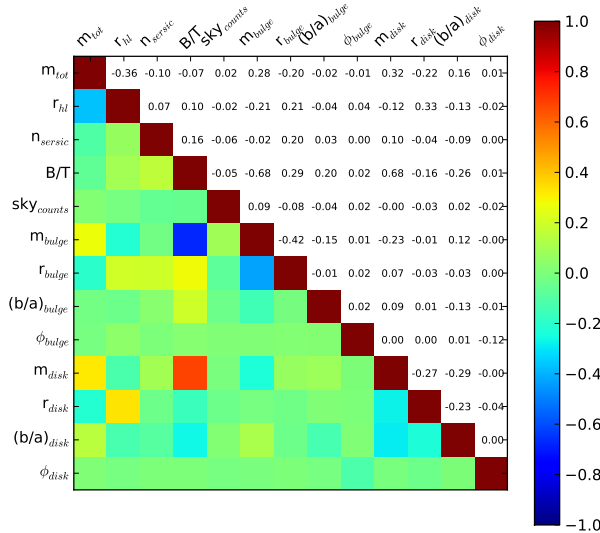
Figure 11. The correlation matrix for a simulated `SerExp` galaxy fit with a `SerExp` model.

Figure 13. The percent difference between the sky estimate of PyMorph for SDSS galaxies and the sky estimated by the SDSS photometric pipeline for those same galaxies. The normalized distribution of differences is shown in bins of 0.1%. A negative difference indicates that the sky measured by PyMorph is lower than that reported by SDSS. The vertical red solid line indicates the median of the distribution. The red dashed, dot-dashed, and dotted lines indicate the 68-95-99% ranges of the data, respectively. The 95% range of sky values is approximately between ±1% difference, so we adopt this as the range used to test the effects of imporper sky estimation.

halflight radius and sky (showing SExtractor sky in blue and our estimates in red) as a function of cutout size. Smaller sizes clearly bias sky estimates made by SExtractor, but only minor improvement in the scatter of any parameters is achieved by using cutout sizes above 20 halflight radii. Since we use SExtractor sky as a starting point for our fitting, we choose a size of 20 halflight radii for our images. The sky estimates of SExtractor improve substantially. However, GALFIT sky estimation is stable over these sizes. Because GALFIT sky estimation is largely independent of the initial starting SExtractor value (which we would expect if we are truly finding the best fit to the galaxy), it is likely the case that cutout sizes smaller than even 10 halflight radii could be used for analysis.

Additional plots of other parameters are omitted in this section. The other fitted parameters show little or no sensitivity to cutout size in the range of cutout sizes used. However, as previously discussed, the bias and scatter may not be equally affected across all model parameters. The effects may be concentrated in a small part of the parameter space.

3.4   The effect of incorrect sky estimation

Estimation of the sky in the vicinity of the target galaxy has a high level of uncertainty. Indeed, accurate sky determination is likely not even a solvable problem as discussed briefly in Blanton et al. (2011). To determine the bias introduced by our sky estimation, we have tested our fitting pipeline in cases of both underestimation and overestimation of the sky. We fix the sky at the simulated sky level, as well as at simulated sky level ±0.5% and ±1.0%. These ranges were chosen to represent the range of differences between our sky estimations and those provided in the CASJOBS database for the SDSS spectroscopic sample.

Figure 13 shows a comparison of sky estimates using PyMorph to those provided from the SDSS photometric data
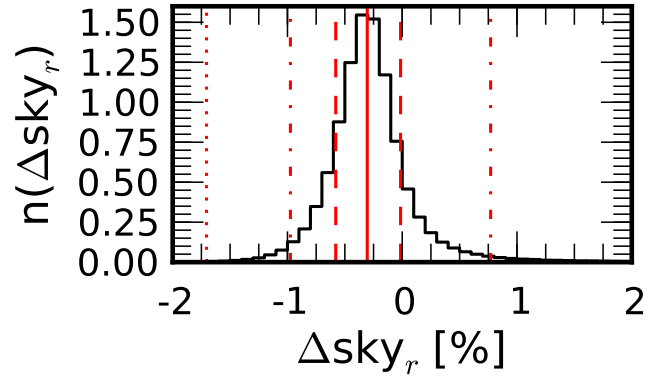
pipeline. This comparison is performed on data from the catalog presented in M2013. The Figure shows the normalized distribution of differences in sky estimation in bins of 0.1%. A negative difference indicates that the sky measured by PyMorph is lower than that reported by SDSS. The vertical red solid line indicates the median of the distribution. The red dashed, dot-dashed, and dotted lines indicate the 68-95-99% ranges of the data, respectively. The 95% range of sky values is approximately between ±1% difference. For the test, we adopt this range as the range to test for sky variation.

The results of incorrectly estimating the sky are shown in Figures 14 and 15. In red, we show the results of fitting galaxies using the standard PyMorph pipeline, treating sky level as a free parameter in the fit. PyMorph systematically underestimates the sky at the 0.1% level. However, the scatter is very tight as indicated by the vertical dashed red lines. In black we have plotted the fitting results at fixed sky levels of the correct value and ±0.5% and ±1.0%. Errors approaching 0.5% clearly introduce a large bias in the fits. The 0.5% level is an important level because it is the approximate level of overestimation shown in the preceding section (section 3.3) found by SExtractor.

Note the asymmetry of the effects of incorrect sky estimation on fitting parameters. In particular, an underestimate of sky is much more detrimental to the fit than the corresponding overestimate, because it can have a substantial effect on fitted halflight radii and Sérsic index. Our pipeline tends to underestimate the sky at the ≈0.1% level which would potentially bias our fits. However, this bias is much smaller than the bias associated with using the SExtractor sky estimate. `SerExp` disk components are remarkably robust to the errors, while bulge paramteres suffer greatly, especially when the sky is underestimated.

Additionally, Figure 13 shows that PyMorph consistently estimates the sky at a level lower than that of the
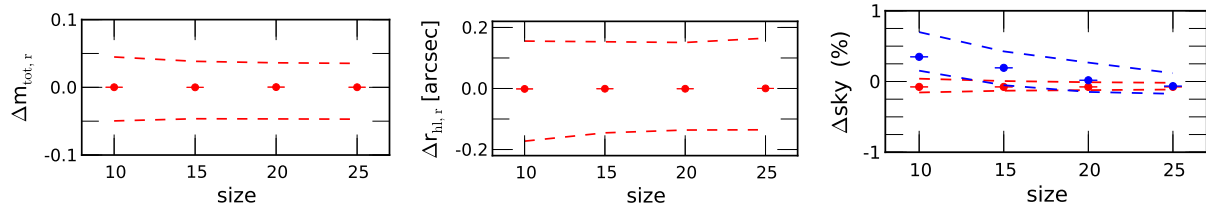
Figure 12. The mean difference of the total magnitude (left column), PSF-corrected halflight radius (center column), and sky estimation (right column) as a function of cutout size for simulated `SerExp` galaxies fitted with a `SerExp` model. Other simulated models behave similarly. For sky estimation, the sky measured by GALFIT is plotted in red. SExtractor sky measurements are plotted in blue for reference. One-σ scatter in the fits is plotted as a dashed line. Improvement in scatter when fitting for cutout sizes above 20 Petrosian Radii is limited, so we use a 20 halflight radii cutout size for all images. Fit parameters seem to have no sensitivity to cutout size in this range, suggesting that it may even be possible to use smaller cutouts.

SDSS pipeline. If we correct the PyMorph estimate of sky by the bias noted from the simulations, we find that PyMorph underestimates sky brightness at the 0.1% level while the difference between the PyMorph sky estimation and the SDSS photometric pipeline is about 0.25%, suggesting that the sky values in SDSS are, in fact, overestimated by approximately 0.15%.

Upon further examination of Figure 15, the bulge parameters of the model are more accurately estimated when the sky is treated as a free parameter in the fit rather than when the sky is fixed at the correct value. The biases discussed in Section 3.1 (i. e., underestimate of the Sérsic index) are partially offset by the biases introduced due to underestimate of the sky. This leads to an apparent improvement in the recovery of fit paramters.

3.5 Testing with real images

To verify the validity of the simulated background and to test the fitting pipeline in clustered environments, we insert the simulated galaxies into real SDSS fpC images. The fpC images are selected from SDSS DR7 images containing spectroscopic galaxy targets to ensure that any environmental changes are minimized.

In Figures 6(c), 7(c), 8(c), 9(c), and 10(c) we show the scatter resulting from fitting the simulated galaxies inserted into real fpC images. The scatter and the bias in the fits remains unchanged, suggesting that we have properly modeled the sky background and neighboring sources common to an SDSS spectroscopic galaxy.

Dense environments provide an additional test for our pipeline. To select fpC images that contain dense environments, we use the GMBCG catalog (Hao et al. 2011). We match cluster BCGs with galaxies in our original catalog to select fpC images with cluster members including the BCG. Our simulated galaxies are then inserted into the image. The simulated galaxy in a clustered environment is then run through the pipeline. In our previous simulations, intracluster light and gradients in the sky were not modeled. These tests allow us to see what the effects may be. Figures 6(d), 7(d), 8(d), 9(d), and 10(d) show the results of the fits. Once again, the errors remain unchanged, showing that no environmental correction is necessary when using the fits from the pipeline.

Placing simulated galaxies near cluster members allows us to test for systematic effects in crowded fields. However, further examination of BCG galaxies is necessary before we are able to properly model them for this purpose. For example, the curvature at the bright end observed in the size-luminosity relation of early-type galaxies (see Bernardi et al. 2012) appears to be due to an increasing incidence of BCGs, which define steeper relations than the bulk of the early-type population (e. g., Bernardi et al. 2007, 2012). However, the curvature could also be due to intracluster light (e. g., Bernardi 2009). Further tests for the largest, brightest galaxies are needed to explore this possibility. We have not presented these tests in this text.

3.6 Testing HST quality images

As a final test, we simulated galaxies using settings similar to HST data for the F850LP filter band using the Advanced Camera for Surveys (ACS). Although similar to testing recovery at higher redshift, the focus is on examining the effects of further lowering the S/N.

Prior to simulation, the sizes and magnitudes of the galaxies are rescaled to the apparent size and magnitude of the same galaxies at a redshift of $z \sim 1.5$. However, proper k-corrections and size corrections are not applied. The pixel size is decreased by a factor of ≈ 10 (from 0.396 to 0.03 arcsec/pixel). Additional adjustments are made to the zero-point and exposure time to properly account for HST-like observing conditions.

For background images, the simulated GEMS tiles are used (for further discussion, see Häussler et al. 2007). Following Häussler et al. (2007), we adopt a hybrid simulation method. Standard HST images typically undersample the PSF and require the use of drizzling to reconstruct the properly sampled image. Nevertheless, we simulate images with the final full resolution (0.03 arcsec/pixel). We add Poisson noise to the simulated image. Then the simulated galaxy is inserted into a simulated image from the GEMS survey. This ensures that the galaxies have noise models similar to real HST images.

These simulations allow us to explore lower S/N fits and the effects on parameter recovery. The S/N as a function of absolute magnitude for the simulations presented in sections 3.1 through 3.5 and this section are compared in Figure 16.

The reduction in S/N increases the scatter without biasing the fits. Examples of the scatter in the total magnitude and halflight radius are plotted in Figure 17. The 68% scatter is increased to $\approx 0.05 - 0.10$ in apparent magnitude
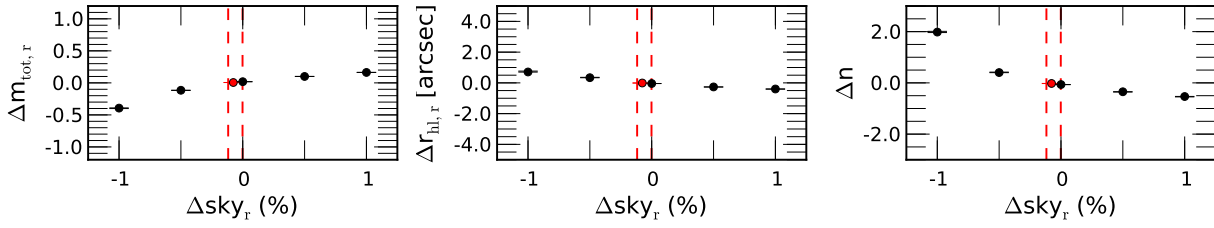
Figure 14. The simulated and recovered apparent magnitude (left), halflight radius (center), and Sérsic index (right) for a `Ser` galaxy fit with a `Ser` model The residuals are plotted as a function of the sky level. Points plotted in black are from fits performed with fixed sky. The overplotted points in red are the result of fitting with sky level as a free parameter in the fit. The vertical dashed red lines mark the 68% scatter of the free sky determination. Our fits are slightly biased low, and this contributes to a small overall bias in fit parameters.
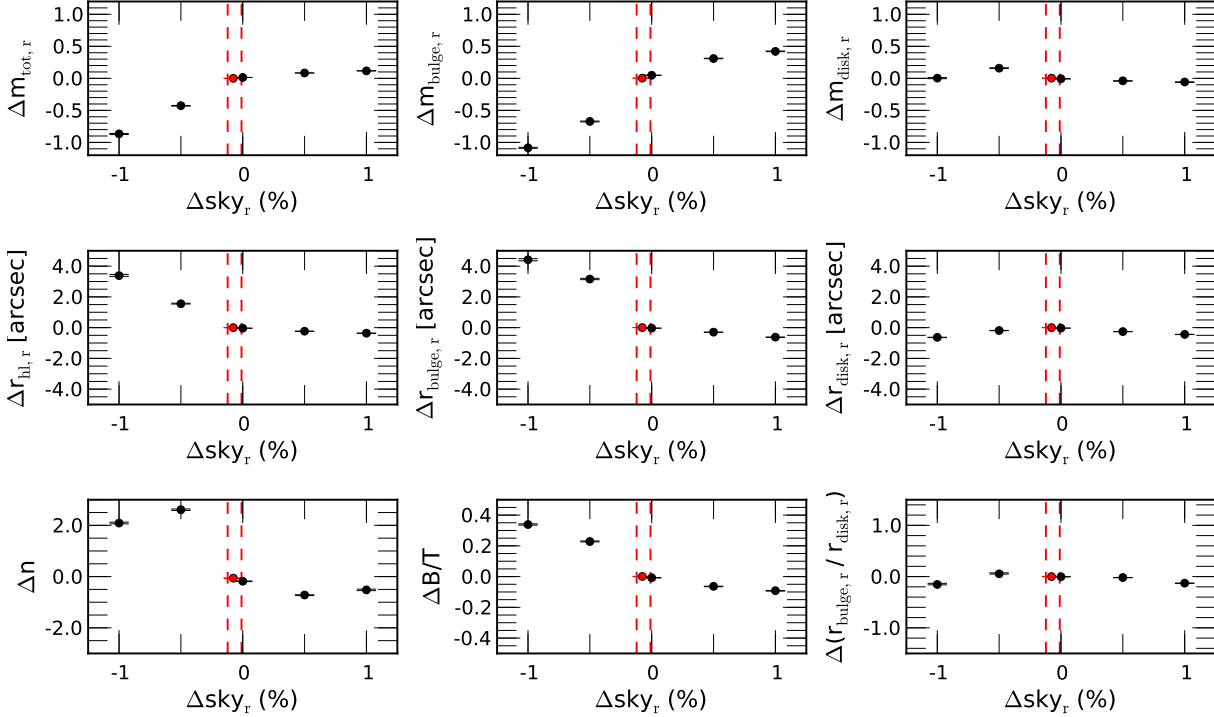
Figure 15. The simulated and recovered parameters of a simulated `SerExp` galaxy fit with a `SerExp` profile. The residuals are plotted as a function of the sky level. Points plotted in black are from fits performed with fixed sky. The overplotted points in red are the result of fitting with sky as a free parameter of the model. The vertical dashed red lines mark the 68% scatter of the GALFIT sky determination. Notice that disk parameters are relatively robust while bulge parameters suffer from incorrect sky estimation. Underestimates of sky level have a particularly strong effect on the bulge.

and ≈ 0.1 arcsec in halflight radii. The dependence of the scatter on magnitude parallels the average S/N vs. apparent magnitude and reflects the sensitivity to S/N that we have referred to throughout the paper. This dependence is also apparent in the scatter of the halflight radius when examined vs. magnitude.

4   DISCUSSION

In the preceding sections we have shown the covariance, bias, and scatter in our parameter estimation for the `Ser` and `SerExp` models. In reality, the effects above will combine to yield a total scatter, covariance, and bias that should approach those shown in 3.2. Our simulations give us an idea of the behavior of the PyMorph pipeline when fitting SDSS galaxies as presented in M2013.

The simulations show that the recovery of global fitting parameters (total magnitude and halflight radius) in the case of SDSS galaxies is remarkably robust, even in the case of the `SerExp` fits. In the case of two-component fits, the bulge component is exhibits systematics. However, the two component fits still provide valuable insight into the structure of galaxies.

Many galaxies exhibit more complex structure than a single or two component structure. Even the case of a two component model often oversimplifies galaxy structure. Bars, rings, central sources, clumpyness, or asymmetry cannot be effectively modeled in our simulations. Because of this, we can only determine a lower-bound on the uncer-
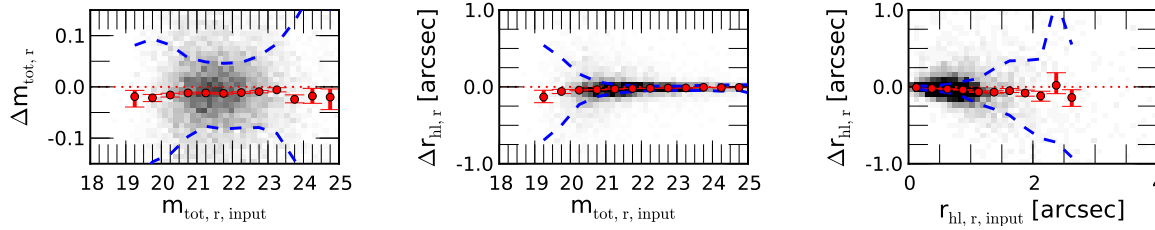
Figure 17. Simulated and recovered magnitude and halflight radius of a simulated `Ser` galaxy fit with a `Ser` profile. Other fits have similar behavior. The scatter in recovered magnitude has increased substantially. The shape of the scatter in the magnitude plot mirrors the behavior of the S/N. Estimation of the halflight radius exhibits less of an effect, and may even improve, likely due to the increased resolution.
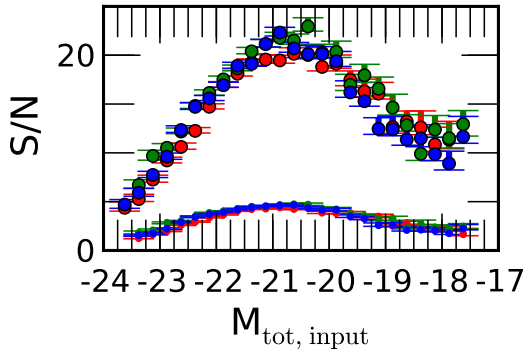

Figure 16. The distribution of galaxy S/N as a function of absolute magnitude for the `Ser` model in red, the `DevExp` model in green, and the `SerExp` model in blue. The median in each bin is shown with symbols. The SDSS galaxies are shown with large filled circles, while the redshifted sample is shown with smaller filled points. The redshifted sample has S/N lower by a factor of ≈ 5.

tainty in our parameter estimates. However, correcting fits using this lower bound represents an improvement in the fits of the observed galaxy. Additionally, the galaxies fit in M2013 have a median size roughly equivalent to the average PSF of SDSS, meaning that, for many galaxies, the resolution necessary to resolve this substructure is not present.

Our tests were performed on r-band data from SDSS. The performance of the pipeline can change when observing in different bands. This change is primarily dependent on the change in the S/N between bands (due to the changing brightness of the sky and the color of the galaxy) and on the different galactic structures to which neighboring SDSS filter bands are sensitive. In M2013, we fit the SDSS g, r, and i band data. It is unlikely that the images change drastically enough over the wavelength and redshift range observed to require additional testing in the g and i bands. However, these simulations become an increasingly poor estimate of error in bluer bands where the photometry becomes more sensitive to star forming regions. These regions tend to be clumpier and, therefore, less well represented by a smooth profile. Therefore, g band fits may present more scatter than the r or i band data.

The question of whether it is possible to perform a two-component fit on data with moderate to low S/N is often presented in light of fits similar to these. When a sample

of galaxy parameters with proper background and S/N are fitted, the resulting fits are indeed robust for many parameters, although specific areas of the parameter space must be treated carefully. In particular, the bulge components of a two component `SerExp` fit suffer from systemmatics, particularly at larger radii and larger Sérsic indexes. However, the bulge and disk parameters are recoverable for a wide range of simulated model parameters. With this information, we can look more seriously at the fits presented in M2013.

The question of which fit is the "correct" fit for any given galaxy is also often asked. To answer this question, one can use the reduced χ^2 for each fit type to test whether a statistically significant change occurs when relaxing the parameters of the model (i. e., going from a one-component to two-component fit, or allowing the Sérsic index to vary) or whether improvement in the fit simply results from more freedom in the model. This comparison was done by Simard et al. (2011). This is certainly a statistically valid question. However, the question of which fit is the most appropriate fit should not be confused with stating that the "incorrect" models do not reveal valid information about the galaxies of interest. In Bernardi et al. (2012), we show that the use of the all the models jointly can often lift degeneracy and reveal important systematic trends in the fitting process.

5 CONCLUSION

We presented the simulations used to test fitting of SDSS galaxies using PyMorph. Simulations of the `Ser` and `SerExp` models were presented and examined in many different cases. The simulations were generated using the results of the fits presented in M2013. We showed that our simulations are recoverable in the case of no noise, which demonstrates that our simulations are correct. We then showed that we can recover the parameters in the case of a simulated background and noise representative of the average SDSS image.

Several individual effects on the fitting were examined. We showed that our choice of 20 halflight radii for cutout size does not significantly bias our fitting results. In addition, we examined the effect of incorrect background estimation, which can significantly affect fitting results.

We also examined the bias created when fitting incorrect models to galaxies. Fitting a two-component Sérsic + Exponential model to what is really just a single Sérsic results in a noisier recovery of the input parameters, but these are not biased; fitting a single Sérsic to what is truly a two-component system results in significant biases. These biases,

for total magnitude and halflight radius in particular, should be useful in correcting other automatic fitting routines.

These simulations can be analyzed together with the fits presented in M2013 to give a more detailed understanding of galaxy structure and formation as presented in Bernardi et al. (2012).

REFERENCES

Abazajian K. N., Adelman-McCarthy J. K., Agüeros M. A., Allam S. S., Allende Prieto C., An D., Anderson K. S. J., Anderson S. F., et al., 2009, ApJS, 182, 543
Bernardi M., 2009, MNRAS, 395, 1491
Bernardi M., Hyde J. B., Sheth R. K., Miller C. J., Nichol R. C., 2007, AJ, 133, 1741
Bernardi M., Meert A., Vikram V., Huertas-Company M., Mei S., Shankar F., Sheth R. K., 2012, MNRAS submitted,
Bertin E., Arnouts S., 1996, A&AS, 117, 393
Blanton M. R., Kazin E., Muna D., Weaver B. A., Price-Whelan A., 2011, AJ, 142, 31
de Vaucouleurs G., 1948, Annales d'Astrophysique, 11, 247
Freeman K. C., 1970, ApJ, 160, 811
Graham A. W., Driver S. P., 2005, PASA, 22, 118
Hao J., Mckay T., Koester B., Rykoff E., Rozo E., Annis J., Wechsler R. H., Evrard A., et al., 2011, in Bulletin of the American Astronomical Society, Vol. 43, American Astronomical Society Meeting Abstracts #217, p. 213.06
Häussler B., McIntosh D. H., Barden M., Bell E. F., Rix H.-W., Borch A., Beckwith S. V. W., Caldwell J. A. R., et al., 2007, ApJS, 172, 615
Huertas-Company M., Shankar F., Mei S., Bernardi M., Aguerri J. A. L., Meert A., Vikram V., 2012, ApJsubmitted,
Kelvin L. S., Driver S. P., Robotham A. S. G., Hill D. T., Alpaslan M., Baldry I. K., Bamford S. P., Bland-Hawthorn J., et al., 2012, MNRAS, 421, 1007
Kent S. M., 1985, ApJS, 59, 115
Lackner C. N., Gunn J. E., 2012, MNRAS, 421, 2277
Meert A., Vikram V., Bernardi M., 2013, In Prep,
Peng C. Y., Ho L. C., Impey C. D., Rix H.-W., 2002, AJ, 124, 266
Press W. H., Teukolsky S. A., Vetterling W. T., Flannery B. P., 1992, Numerical recipes in C. The art of scientific computing
Sérsic J. L., 1963, Boletin de la Asociacion Argentina de Astronomia La Plata Argentina, 6, 99
Shankar F., Marulli F., Bernardi M., Mei S., Meert A., Vikram V., 2012, MNRAS, 1
Simard L., Mendel J. T., Patton D. R., Ellison S. L., McConnachie A. W., 2011, ApJS, 196, 11
Vikram V., Wadadekar Y., Kembhavi A. K., Vijayagovindan G. V., 2010, MNRAS, 409, 1379